Estimation of frequency-wavenumber diagrams using a physics-based grid-free compressed sensing method

Thomas Paviet-Salomon, Julien Bonnel *Member, IEEE*, Clément Dorffer, Barbara Nicolas *Member, IEEE*, Thierry Chonavel, Dag Tollefsen, David P. Knobles, Preston S. Wilson, Angélique Drémeau

Abstract

Shallow water propagation can be described using modal theory. For low frequency sources, propagated signals are composed of a few dispersive modes, each of them propagating with its own frequency-dependent wavenumber. Modal estimation, and particularly wavenumber estimation, is of great interest in seabed characterization but classically requires a large and dense horizontal line array (HLA). The compressed sensing (CS) paradigm, which allows one to reduce the number of sensors, has been used to overcome this limitation. However, CS performance is directly linked to the discrete basis used in the process and is known to degrade with basis mismatch. To mitigate this issue, the current paper proposes a physics-based grid-free approach to perform wavenumber estimation using a HLA with a limited number of sensors and a single broadband source. The proposed method has three main features: it starts with a speed correction to prevent wavenumber aliasing (using water sound speed at the array location), it then embeds physical prior (the modal dispersion relation) at the core of the CS framework, and it involves a CS grid-free approach. The performance of the method is quantified on simulated data using the Jaccard's distance. It has been applied successfully on experimental data from the 2017 Seabed Characterization Experiment.

Index Terms

Underwater acoustics, compressed sensing, normal mode propagation, Seabed Characterization Experiment, SBCEX17.

T. Paviet-Salomon, C. Dorffer and A. Dremeau are with Lab-STICC, ENSTA Bretagne, UMR CNRS 6285, Brest, France (e-mail: angelique.dremeau@ensta-bretagne.fr,clement.dorffer@ensta-bretagne.fr,thomas.paviet-salomon@ensta-bretagne.org). J. Bonnel is with the Applied Ocean Physics and Engineering Department, Woods Hole Oceanographic Institution, Woods Hole, Massachusetts 02543, USA (e-mail: jbonnel@whoi.edu). B. Nicolas is with Univ Lyon, INSA-Lyon, UJM-Saint Etienne, CNRS, Inserm, Creatis UMR 5220, U1206, F-69601, Lyon, France. T. Chonavel is with Lab-STICC, IMT Atlantique, UMR CNRS 6285, Brest, France (thierry.chonavel@imt-atlantique.fr). D. Tollefsen is with the Norwegian Defence Research Establishment (FFI), Defence Systems Division, Horten NO-3191, Norway (e-mail: dag.tollefsen@ffi.no). P. Wilson is with The Walker Department of Mechanical Engineering & Applied Research Laboratories, University of Texas at Austin, Austin, Texas 78712, USA (e-mail: pswilson@mail.utexas.edu). D. Knobles is with Knobles Scientific and Analysis, LLC, Austin, Texas 78731, USA (e-mail: dpknobles@kphysics.org)

I. INTRODUCTION

In shallow-water environments (water depth $D < 200$ m), the acoustic propagation of a low-frequency ($f < 100$ Hz) signal is conveniently described by normal mode theory. Under this assumption, the signal is modeled by the sum of a small number of propagating modes (less than ten in this work). The modes are fully characterized by their frequency-dependent wavenumbers and amplitudes. These two modal features have been extensively used as input data for inverse problems, such as source localization [1], [2] and/or environmental estimation [3], [4]. As a result, modal estimation is an important topic for ocean acoustics. The present paper focuses on modal wavenumber estimation.

When range aperture is available, wavenumber estimation is similar to spectral analysis in the spatial dimension. Assuming that the signal is collected on a long horizontal line array (HLA) with a source in the endfire direction, the easiest way to estimate the wavenumber spectrum is to compute a spatial Fourier transform (SFT) in the horizontal dimension. Further, if the source is broadband, one can also compute a second Fourier transform in the temporal dimension (TFT) to obtain a frequency-wavenumber (f-k) diagram, which fully characterizes modal dispersion [5], [6].

The main drawback of this simple procedure is that it suffers from the traditional limitations of the Fourier-based spectral analysis. In our context, a large horizontal aperture and a large number of sensors (i.e. a long and dense HLA) are required to properly resolve the modal wavenumbers. To mitigate this issue, the SFT can be replaced by more advanced spectral estimation methods. Pioneer studies successfully replaced the SFT with an auto-regressive (AR) estimator [7], [8]. Since the propagation in shallow-water environments is described by a small number of modes, considering sparse models constitutes an interesting alternative. These models are in particular involved in the compressed sensing (CS) paradigm [9] which, as it will be emphasized in the following, is of particular interest here, but has been more broadly exploited in underwater acoustics (e.g. [10], [11]). CS has first been used to estimate modal wavenumber in ocean acoustics by Le Courtois et al. [12]. Interestingly, CS has also been used to estimate modal wavenumber in other scientific fields, e.g. structural health monitoring using Lamb waves [13], [14]. A special issue of the Journal of The Acoustical Society of America is dedicated to CS in acoustics, and the editorial introduction [15] includes a comprehensive review of CS.

Traditionally, CS algorithms expand the signal on the elements of a finite basis, i.e. a discrete grid. When the components of the signal do not match the grid, basis mismatch occurs, which degrades the CS performances [16]. Off-grid CS approaches have been proposed to mitigate this issue [17], [18]. They have been notably applied to underwater acoustic problems, such as plane wave beamforming [19] or modal estimation using a vertical line array (VLA) and a source at multiple ranges [20]. Later, Paviet-

Salomon et al. [21] proposed to use grid-free CS to perform modal wavenumber estimation using a single broadband source and a small number of sensors. As in Ref. [22], the authors further embedded a physical assumption, the *dispersion relation*, within the CS framework to relate wavenumbers from one (temporal) frequency to the next. The method was successfully validated on data simulated in a Pekeris waveguide [21].

In the present article, we extend the work of Paviet-Salomon et al. [21]. The method is improved by implementing a frequency-dependent shift of the wavenumber spectra. This processing, which effectively creates an equivalent baseband version of the spatial signal thanks to a speed correction, is traditionally used for seismic applications [5], [6]. Here, it prevents wavenumber aliasing and thus allows wavenumber estimation over a relatively wide frequency band. On the other hand it modifies the dispersion relation that is used at the core of the CS framework.

In the present work, the performance of the proposed method is benchmarked on realistic simulations, and shown to be superior to the state of the art. The method is also applied on experimental marine data collected during the 2017 Seabed Characterization Experiment (SBCEX17) [23]. This article considers a combustive sound source (CSS) signal recorded on a HLA with an aperture of 1 km. The proposed method allows the estimation of the wavenumbers of the four first modes from 10 Hz to 100 Hz using as few as 10 sensors. These experimental results, obtained on SBCEX17 data collected on the New England Mud Patch, illustrate the method's robustness to complex environments with vertical stratification. Indeed, the New England Mud Patch features a complex layered seafloor. It notably has a layer of mud whose upper part is believed to be slower than water [24], [25], which clearly impacts the propagating modes [26].

The remainder of the paper is organized as follows. Section II briefly introduces modal propagation, and focuses on the dispersion relation which will be at the core of the proposed method. Section III reviews the CS framework. It then describes on-grid and off-grid methods. Section IV presents the proposed wavenumber estimation procedure. First, Sec. IV-A reviews speed correction, a process that prevents wavenumber aliasing. Then, Sec. IV-B details the physics-based grid-free wavenumber tracking algorithm. Lastly, Sec IV-C introduces the Jaccard distance, a suitable metric to assess the performances of the method. Applications are presented in Sec. V, which cover a simulated benchmark and comparison with the state-of-the-art, as well as experimental results obtained using data from the 2017 Seabed Characterization Experiment. Section VI summarizes and concludes the article.

II. Acoustic propagation in dispersive shallow water environments

A. Received signal

This paper focuses on low-frequency ($f < 100$ Hz) acoustic propagation in shallow water ($D < 200$ m). In this context, as stated in Sec. I, the propagation is described by the modal theory. Consider a frequency-domain signal $s(f)$ emitted by a source at depth at z_s. The received pressure on a sensor located at the distance r and depth z can be written as [27, Chap 5]:

$$y(f,r) \simeq Q \frac{s(f)}{\sqrt{r}} \sum_{m=1}^{M(f)} A_m(f, z_s, z) e^{-jrk_{rm}(f)} + n(f,r), \tag{1}$$

where Q is a constant factor, $M(f)$ is the number of propagating modes at frequency f, $k_{rm}(f)$ is the horizontal wavenumber of the m^{th} mode, and $A_m(f, z_s, z)$ is its amplitude. The quantity $n(f,r)$ stands for the TFT of the measurement noise. Modal attenuation is usually included in Eq. (1) as the imaginary part of k_{rm}. Here, the associated term $e^{-r\Im[k_{rm}(f)]}$ is included in A_m, so that k_{rm} can be considered a real number.

We consider a HLA and a source in the endfire direction (i.e. the source is aligned with the array). The geometrical attenuation factor $1/\sqrt{r}$ in Eq. (1) can be compensated for if the source position is known. As a result, the only significant range-dependence in Eq. (1) is within the phase of the modes. Note that this is still a fair assumption even if the source position is unknown, as long as it is in the endfire direction. Indeed, most of the range variability in Eq. (1) is driven by the complex exponential $e^{-jrk_{rm}(f)}$, and the $1/\sqrt{r}$ can be considered as constant along the HLA, provided that the source/array distance is large enough. As a result $y(f,k)$, the SFT of $y(f,r)$, provides a direct measurement of the wavenumber spectrum (i.e. with peaks at $k_{rm}(f)$). For a broadband source, $y(f,k)$ is called a f-k diagram [5]. Figure 1 presents a simulated f-k diagram. The simulation has been run for a Pekeris waveguide representative of a classical shallow water scenario. For consistency, the environmental parameters are the same as those used in Refs. [21], [22]: water depth $D = 130$ m, sound speed $c_{water} = 1500$ m/s and density $\rho_{water} = 1$ g/cm^3; basement sound speed $c_{bas} = 2000$ m/s and density $\rho_{bas} = 2$ g/cm^3. The f-k diagram was obtained using the FT of data simulated on a long and dense HLA with 240 regularly spaced sensors, with sensor spacing $\Delta r = 25$ m (the array length is nearly 6 km).

B. Dispersion relation

In any environment, the horizontal wavenumbers k_{rm} are linked to their vertical counterparts k_{zm} by the *dispersion relation*. At a given frequency f, this relation is

$$\left(\frac{2\pi f}{c}\right)^2 = k_{rm}(f)^2 + k_{zm}(f)^2, \tag{2}$$

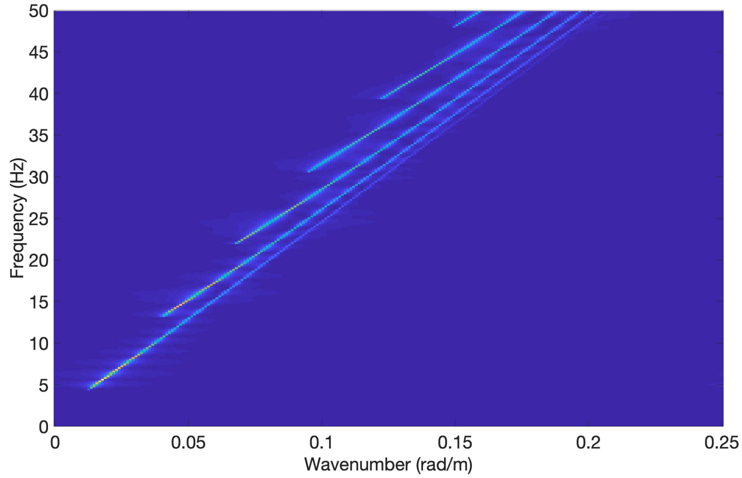

Fig. 1. Simulated f-k diagram in a Pekeris waveguide.

where c is the speed of the sound. Note that in theory, both $k_{zm}(f)$ and c are depth dependent. This is ignored here, as was done in previous studies [21], [22], [28] that use the dispersion relation to guide modal estimation. Indeed, the potential impact of this assumption is small enough that it can be embedded into noise and/or other uncertainties.

As suggested by Le Courtois and Bonnel [12], one can discretize the frequency axis (with $f = \nu\Delta_f$, $\nu \in \mathbb{N}$ and Δ_f the size of a frequency bin) and relate the wavenumbers attached to two successive frequency indices using

$$k_{rm}[\nu+1]^2 = k_{rm}[\nu]^2 + (2\nu+1)\left(\frac{2\pi\Delta_f}{c}\right)^2 + \epsilon[\nu], \tag{3}$$

where $k_{rm}[\nu] = k_{rm}(\nu\Delta_f)$ and $\epsilon[\nu] = k_{zm}[\nu+1]^2 - k_{zm}[\nu]^2$.

In shallow-water environments, the vertical wavenumbers k_{zm} weakly depend on the frequency [27, Chap. 5]. As a result, the quantity ϵ is smaller than the other terms of the equation and can be neglected. This hypothesis has successfully been used in previous studies that took advantage of Eq. (3) at the core of modal estimation scheme [21], [22], [28]. In the present paper, Eq. (3) will be used as a physical prior to enhance wavenumber recovery using an off-grid CS algorithm.

III. Compressed sensing

A. Sparse representation

Using the discretized framework presented in Sec. II-B, we further assume that the received signal has been measured on a HLA with L elements. The received signal $y(f, r)$ is now denoted using $\mathbf{y}_\nu$, a column vector of size L. Assuming that the horizontal wavenumber space is discretized into a grid of size N, Eq. (1) can be expressed as

$$\mathbf{y}_\nu = \mathbf{D}\mathbf{a}_\nu + \mathbf{n}_\nu, \tag{4}$$

where $\mathbf{D} \in \mathbb{C}^{L\times N}$ is a dictionary made up of (spatial) Fourier component, $\mathbf{a}_\nu \in \mathbb{C}^N$ is the wavenumber spectrum at the (temporal) frequency ν (i.e. the transposed version of the ν^{th} line of the f-k diagram of interest) and $\mathbf{n}_\nu \in \mathbb{C}^L$ is the additive noise along the HLA. The $(l,n)^{\text{th}}$ element of $\mathbf{D}$ is defined as $d_{ln} = e^{-jr_l\kappa_n}$, where r_l is the distance between the l^{th} sensor and the source, and κ_n is the n^{th} element of the wavenumber search grid. Note that Eq. (4) requires knowledge about the HLA configuration (i.e. sensor spacing), but does not require the source/array distance to be known, provided that the source is at the endfire direction. In this case, r_l can be referenced to the first sensor of the HLA (i.e. $r_1 = 0$). The resulting solution is similar to the one obtained using the absolute source/array distance, up to a multiplicative phase shift. Note that the n^{th} column of $\mathbf{D}$ will be noted $\mathbf{d}_{\kappa_n}$ hereinafter, i.e. $\mathbf{d}_{\kappa_n} = [1, \ldots, e^{-jr_L\kappa_n}]^T$.

The discrete wavenumber spectrum $\mathbf{a}_\nu$ can be estimated through the SFT of $\mathbf{y}_\nu$, which is equivalent to a least-squares estimation process. However, since the number of propagating modes is small, most of the elements of $\mathbf{a}_\nu$ are null. As a result, the use of sparse recovery (SR) is well adapted to estimate $\mathbf{a}_\nu$ [12], [22]. Within this framework, $\mathbf{D}$ is seen as an overcomplete dictionary (i.e. $L \ll N$) while $\mathbf{a}_\nu$ contains many zero entries. The corresponding SR problem can be expressed as

$$\hat{\mathbf{a}}_\nu = \underset{\mathbf{a}_\nu}{\text{argmin}} \; \|\mathbf{y}_\nu - \mathbf{D}\mathbf{a}_\nu\|_2^2, \text{ subject to } \|\mathbf{a}_\nu\|_0 \le M_\nu, \tag{5}$$

with $||\mathbf{a}_\nu||_0$ the l_0 pseudo-norm of $\mathbf{a}_\nu$ which simply counts the number of non-zero entries of $\mathbf{a}_\nu$ and M_ν the maximum number of modes expected to propagate at frequency ν.

B. On-grid CS algorithm

Eq. (5) is a combinatorial problem, and many heuristic methods have been developed to solve it. They can roughly be divided into three families. A first group of methods replaces the l_0-norm by a l_p-norm (with $0 < p \le 1$). This leads to a relaxed problem which can be solved efficiently by standard optimization procedures. A well-known approach is the Basis Pursuit (BP) [29]. A second group of methods are greedy algorithms which build up the sparse vector $\mathbf{a}_\nu$ from successive greedy decisions. One of the most popular versions of such algorithms is Orthogonal Matching Pursuit (OMP) [30]. The last group of methods are Bayesian algorithms that express the sparse representation as the solution of a Bayesian inference problem. Different Bayesian methods consider different prior models, estimation problems and statistical tools to solve them [31], [32].

Various on-grid CS methods have been used to estimate wavenumbers in ocean acoustics, including an iterative reweighted least squares method [12] and two Bayesian approaches [22], [28]. Interestingly, the two Bayesian approaches [22], [28] use the dispersion relation Eq. (3) to connect horizontal wavenumbers from one frequency to the next. However, Ref. [28] assumes that the number of modes is constant over the bandwidth of interest and that the $\epsilon[\nu]$ term in Eq. (3) can be fully neglected. These two assumptions restrict the modal recovery to a limited bandwith (in [28], the provided examples were limited to a 20 Hz bandwidth, which kept the number of modes constant). On the other hand, Ref. [22] also uses Eq. (3) with $\epsilon[\nu] = 0$ to predict wavenumber at frequency $\nu + 1$, but it introduces freedom around the predictions to account for $\epsilon[\nu] \neq 0$. The associated drawback is that the method includes several parameters that must be tuned by hand.

In the present article, we consider an off-grid CS method that also relies on the dispersion relation Eq. (3). We will later see that the proposed method enables tracking the wavenumbers over a relatively wide bandwidth, while the number of modes does not need to be known *a priori*. Before that, traditional off-grid CS is briefly presented.

C. *Off-grid CS algorithm*

On-grid CS methods have known limitations that notably occur when the non-zero coefficients of $\mathbf{a}_\nu$ do not match the grid points. This issue, called basis-mismatch [33], [16], can be mitigated by using a very fine grid. However, this raises questions about the coherence of the grid (which in turns impacts CS performance) and also may induce numerical instabilities.

These concerns led to the development of grid-free setting methods. Practically, a grid-free version of the relaxed version of Eq. (5) can be obtained by replacing the l_1-norm (only valid in a finite dimensional setting) by the total variation norm [34]. Although the underlying theory is complex, off-the-shelf toolboxes such as the CVX software (ConVeX: a library for convex optimization) [35] are available to solve the problem. This approach was notably used to estimate wavenumbers (and modal depth functions) considering a VLA and a source at multiple ranges [20]. However, the main drawback of this procedure is its high computational cost.

Simultaneously, a continuous version of OMP has been proposed in [17] while a continuous version of BP has been proposed in Ref. [36]. The approach is based on the idea of interpolating the dictionary components between existing grid points. However, an expensive computational cost is still associated with those methods. Rather, we will use a traditional OMP method, coupled with gradient descent performed after each OMP step [37]. The main advantage of this method is to obtain a continuous behavior while being simple, it barely increases the computational cost of the considered SR method. It was previously used in our context (estimation of modal wavenumbers with a HLA) on data simulated in a Pekeris waveguide [21].

Particularized to the mode estimation problem, at each iteration of OMP, two successive operations are performed for a given frequency bin ν :

1) selection of the most correlated atom (or column) in dictionary $\mathbf{D}$ with the current residual $\mathbf{r}_\nu$ (namely the observations minus the current mode estimated contributions),

$$\hat{\kappa}_n = \underset{\kappa_n}{\operatorname{argmax}} |\langle \mathbf{r}_\nu, \mathbf{d}_{\kappa_n} \rangle| \tag{6}$$

where $\mathbf{d}_{\kappa_n}$ is the n-th column of $\mathbf{D}$;

2) estimation of the modal contributions by solving a least-squares estimation on the basis of the current set of selected atoms, denoted as $\mathcal{S}_\nu$:

$$\hat{\mathbf{a}}_{\nu,\mathcal{S}_\nu} = \mathbf{D}^{+}_{\mathcal{S}_\nu} \mathbf{y}_\nu, \tag{7}$$

where $\mathbf{a}_{\nu,\mathcal{S}_\nu}$ (resp. $\mathbf{D}_{\mathcal{S}_\nu}$) stands for the restriction of $\mathbf{a}_\nu$ (resp. $\mathbf{D}$) to the elements (resp. columns) indexed by $\mathcal{S}_\nu$ and $.^{+}$ denotes the Moore-Penrose pseudo-inverse matrix.

An intuitive off-grid estimation can then be obtained by adding a gradient descent procedure between these two steps. Formally, the operation solves the problem :

$$\hat{k}_{rm}[\nu] = \underset{\kappa}{\operatorname{argmax}} |\langle \mathbf{r}_\nu, \mathbf{d}(\kappa) \rangle| = \underset{\kappa}{\operatorname{argmin}}\ J(\kappa) \tag{8}$$

where $\mathbf{d}(\kappa)$ is explicitly written as a function of a continuous variable κ such as $\mathbf{d}(\kappa) = [1, \ldots, e^{-jr_L\kappa}]$. The procedure is iterative and builds on a current estimate at each iteration :

$$\hat{k}^{(\ell)}_{rm}[\nu] = \hat{k}^{(\ell-1)}_{rm}[\nu] - \zeta \nabla J(\hat{k}^{(\ell-1)}_{rm}[\nu]), \tag{9}$$

where ζ is the gradient-descent step, $\nabla J(\hat{k}^{(\ell-1)}_{rm[\nu]})$ is the gradient of $J(\kappa) = -|\langle \mathbf{r}_\nu, \mathbf{d}(\kappa) \rangle|$ estimated for $\kappa = \hat{k}^{(\ell-1)}_{rm}[\nu]$. Coupled with OMP, the gradient descent is initialized at the value of the selected atom in step (1) and results in a new estimate $\hat{k}_{rm}[\nu]$. This new estimate is incorporated in set $\mathcal{S}_\nu$ to be used in the least-squares estimation of step (2). In the following, an additional constraint on the gradient descent is proposed that bounds the estimation into a given search interval. This can be simply implemented using linear regularizations (see [38]) to be taken into account in the definition of $J(\kappa)$. The regularizations being linear, the above procedure remains valid.

IV. Wavenumber estimation

This section describes the proposed method to estimate modal wavenumbers. A modified dispersion relation that will be used within the CS framework is first presented.

A. *Dispersion relation after speed correction*

In any waveguide, the modal wavenumbers are known to be contained within the interval $[\frac{2\pi f}{c_{\max}}, \frac{2\pi f}{c_{\min}}]$, where $c_{\max}$ and $c_{\min}$ are the maximal and minimal sound speed in the environment [27, Chap. 5]. At any frequency, the wavenumber support of the signal is limited to a relatively narrow (wavenumber) band: the spatial signal is said to be a bandpass signal. A small sensor spacing is thus required to prevent wavenumber aliasing. An example of an aliased f-k diagram is presented in Fig. 2a. The simulated environment is the same as in Fig. 1, except that the frequency now goes up to 200 Hz. One can see that above 60 Hz, wavenumbers are aliased. This is because for $f > 60$ Hz, the maximal wavenumber value $\frac{2\pi f}{c_{\min}}$ is above the (spatial) Nyquist frequency $k_s = \frac{1}{2\Delta r}$, with Δr the (spatial) sampling rate (i.e. the sensor spacing).

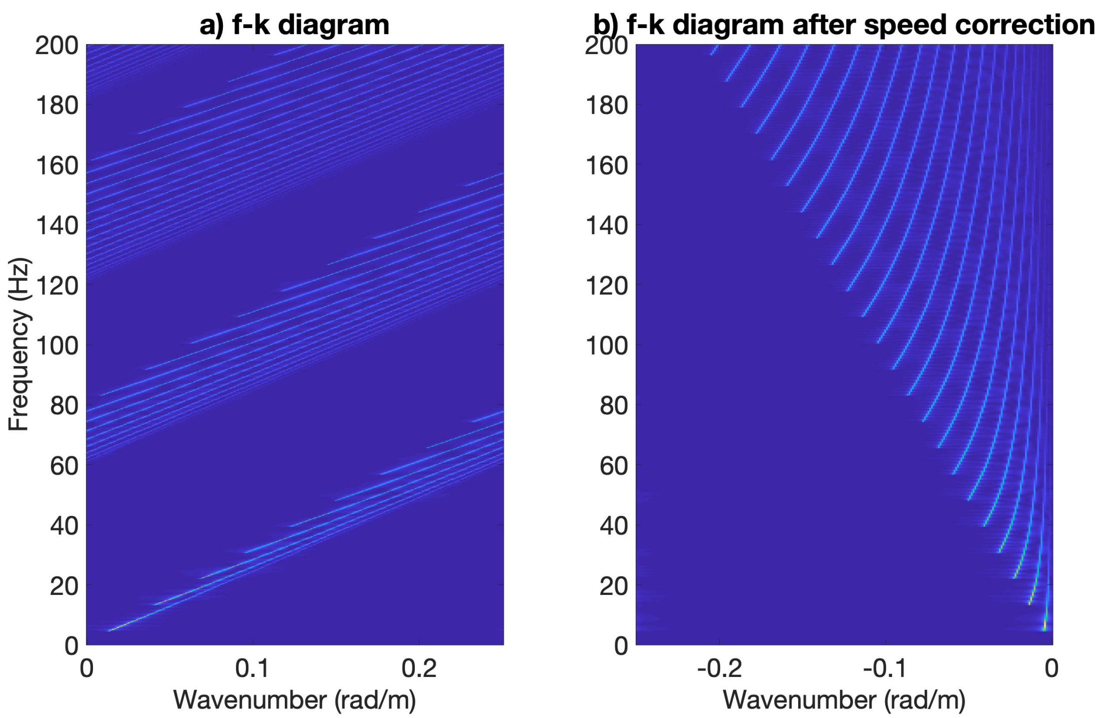

Fig. 2. a) : Frequency-wavevumber diagram in the same configuration as in Fig. 1, except that frequency goes to 200 Hz: wavenumber are aliased for $f > 60$ Hz. b) : f-k diagram in the same configuration, but after speed correction: there is no aliasing.

Aliasing can be prevented by reducing the spacing between sensors, but this is not always possible at sea. Since the wavenumber spectrum is a bandpass signal, aliasing can also be prevented by translating the modal spectrum toward smaller wavenumbers (i.e. baseband processing). Mathematically, this is done by time-shifting the received data using $c_{\min}$ sound speed, which in the frequency domain corresponds to

$$\tilde{y}(f,r) = e^{\left(jr\frac{2\pi f}{c_{\min}}\right)} y(f,r), \tag{10}$$

with $\tilde{y}(f,r)$ the shifted signal. The wavenumber support of $\tilde{y}$ becomes $[\frac{2\pi f}{c_{\max}} - \frac{2\pi f}{c_{\min}}, 0]$, which drastically reduces the Nyquist frequency. This process is common in geophysics [5], [39], [40] and has also found applications in ocean acoustics [6], [41]. It will be called speed correction hereafter. Speed correction is applied on the simulated Pekeris example, and the result is presented in Fig. 2b. One can see that wavenumbers can now be recovered without aliasing up to 200 Hz.

Although the speed correction process is simple, it modifies the dispersion relation. The original wavenumbers $k_{rm}[\nu]$ and their shifted versions $\tilde{k}_{rm}[\nu]$ are linked through

$$k_{rm}[\nu] = \tilde{k}_{rm}[\nu] + \gamma\nu, \tag{11}$$

with $\gamma = \frac{2\pi\Delta_f}{c_{\min}}$. Using Eq. (11) into Eq. (3), the discretized dispersion relation becomes

$$(\tilde{k}_{rm}[\nu+1] + \gamma(\nu+1))^2 = (\tilde{k}_{rm}[\nu] + \gamma\nu)^2 + (2\nu+1)\gamma^2 + \epsilon[\nu]. \tag{12}$$

Assuming that $\epsilon[\nu] = 0$, the wavenumber at frequency $\nu + 1$ can be predicted using

$$\tilde{k}_{rm}^{\text{pred}}[\nu+1] = -\gamma(\nu+1) + \sqrt{(\tilde{k}_{rm}[\nu] + \gamma\nu)^2 + (2\nu+1)\gamma^2}. \tag{13}$$

Note that in the proposed method, the (incorrect) assumption $\epsilon[\nu] = 0$ will be mitigated by looking for wavenumbers in a small interval centered around the predicted value $\tilde{k}_{rm}^{\text{pred}}[\nu+1]$.

B. Tracking modes

As stated in the introduction, the tracking method proposed in this article is largely similar to the one in [21]. The only difference is that we now work after speed correction. As a result, the physical prior that is embedded into the grid-free CS algorithm is now Eq. (12), instead of Eq. (3). This enables tracking wavenumbers in configurations where sensor spacing is large and creates wavenumber aliasing. In such situation, the method from [21] cannot be used. Note that if sensor spacing is small enough to prevent aliasing without speed correction, then the proposed method gives result similar to the method in [21]. The proposed method is summarized below.

The proposed procedure starts at $\nu = 1$ with a traditional OMP step, evaluating the most correlated atom of the dictionary $\mathbf{D}$ with the signal $\mathbf{y}_\nu$. This step is then completed by a detection operation, which compares the resulting correlation to a given threshold T_0. If selected, a mode is considered to propagate and the dispersion relation (12) is used to predict the interval in which the wavenumber of this mode is likely to be at the next frequency. The current estimate, as well as the predicted wavenumber at the next frequency, is then refined by a gradient-descent step, respectively based on the selected atom and within the predicted interval. For the predicted wavenumber of mode m at the next frequency $\nu+1$, a detection threshold $T_{m,\nu+1}$ is again applied on its estimated amplitude to prevent the propagation of false alarms. All these steps are then repeated at the next frequency in order to detect possible new modes and to propagate those already predicted to higher frequencies.

The overall procedure is summarized in the Algorithm 1. An important parameter is ξ in Eq. (15): it gives the algorithm freedom to look for $\tilde{k}_{rm}[\nu+1]$ around the predicted value $\tilde{k}_{rm}^{\mathrm{pred}}[\nu+1]$. In a given context, the value of ξ is empirically determined by simulations to maximize the method's performances.

Algorithm 1 Physics-based grid-free Orthogonal Matching Pursuit for data with speed correction.

input $\forall \nu \in \{1,..,F\}$, $\mathbf{r}_\nu = \mathbf{y}_\nu$, $\mathcal{S}_\nu = \emptyset$, $I_{0,\nu} = \emptyset$, $M=0$.

for $\nu = 1 : F$ **do**

while stopping criteria is not reached **do**

$\mathbf{1}$. If $M \geq 1$, propagate existing modes

For $m = 1 : M$

– Apply gradient descent on interval $I_{m,\nu}$ and get $\hat{k}_{rm}[\nu]$. If $|\langle \mathbf{r}_\nu, \mathbf{d}_{\hat{k}_{rm}[\nu]} \rangle| \geq T_{m,\nu}$, set $\mathcal{S}_\nu = \mathcal{S}_\nu \cup \hat{k}_{rm}[\nu]$.

– Compute corresponding coefficients and update residual : $\mathbf{r}_\nu = \mathbf{y}_\nu - \mathbf{D}_{\mathcal{S}_\nu} \hat{\mathbf{a}}_{\nu,\mathcal{S}_\nu}$ with $\hat{\mathbf{a}}_{\nu,\mathcal{S}_\nu} = \mathbf{D}_{\mathcal{S}_\nu}^{+} \mathbf{y}_\nu$.

$\mathbf{2}$. Find new propagating wavenumber

$$\hat{\kappa}_n = \underset{\kappa_n}{\operatorname{argmax}} |\langle \mathbf{r}_\nu, \tilde{\mathbf{d}}_{\kappa_n} \rangle|, \tag{14}$$

where $\tilde{\mathbf{d}}_{\kappa_n}$ is the n-th column of $\mathbf{D}_{(\cup_{m\in\{0,\dots,M\}} I_{m,\nu})^C}$ made up of Fourier atoms not in $\cup_{m\in\{0,\dots,M\}} I_{m,\nu}$.

If $|\langle \mathbf{r}_\nu, \tilde{\mathbf{d}}_{\hat{\kappa}_n} \rangle| \geq T_0$

– Set $M = M+1$.

– Apply gradient-descent procedure to refine previous estimate and get $\hat{k}_{rm}[\nu]$. Set $\mathcal{S}_\nu = \mathcal{S}_\nu \cup \hat{k}_{rm}[\nu]$.

– Compute corresponding coefficients and update residual : $\mathbf{r}_\nu = \mathbf{y}_\nu - \mathbf{D}_{\mathcal{S}_\nu} \hat{\mathbf{a}}_{\nu,\mathcal{S}_\nu}$ with $\hat{\mathbf{a}}_{\nu,\mathcal{S}_\nu} = \mathbf{D}_{\mathcal{S}_\nu}^{+} \mathbf{y}_\nu$.

$\mathbf{3}$. Predict propagating intervals for next frequency

For all $m \in \{1, \dots, M\}$, define

$$I_{m,\nu+1} = \left[\tilde{k}_{rm}^{\mathrm{pred}}[\nu+1] - \xi; \tilde{k}_{rm}^{\mathrm{pred}}[\nu+1] + \xi\right]. \tag{15}$$

end while

end for

Detection thresholds may depend on false alarm probabilities. More particularly, considering a Gaussian complex circular noise assumption with variance σ^2, we can define T_0 as

$$T_0 = \sigma\sqrt{-2\log\beta_0} \tag{16}$$

where β_0 is a given false alarm probability considered for the detection of a new mode. We adopt a similar definition for $T_{m,\nu}$, but we add further physical considerations. If a mode m is detected first at frequency $\nu_{c,m}$ with threshold T_0, we know that the mode will still be present at higher frequencies, suggesting thus to decrease the threshold for increasing frequencies. This can be done by considering:

$$T_{m,\nu} = T_0 - \sum_{i=1}^{\nu-\nu_{c,m}} \left(\frac{1 - \frac{T_\infty}{T_0}}{2 - \frac{T_\infty}{T_0}} \right)^i T_0, \tag{17}$$

where $T_\infty = \sigma\sqrt{-2\log\beta_\infty}$ stands for a desired limit threshold depending on an asymptotic false alarm probability β_∞ under the same Gaussian complex circular noise assumption. More details on the adopted strategy with regard to these thresholds can be found in [21].

C. *Performance of the algorithm : the Jaccard distance*

An interesting question arises in quantifying the performance of the proposed method. Since the mode number is not known *a priori*, it is important to account for mismatch between the estimated number of modes, the true number of modes, and the fact that this number may vary with frequency. As a result, the problem can be seen as the detection and tracking of an unknown number of targets. A relevant metric in this context is the Jaccard distance [18], [42], [43].

The Jaccard distance D_J is built using traditional detection theory features: the true positive (TP), false negative (FN) and false positive (FP) rates. Here, the quantities TP, FN and FP are evaluated at every frequency of interest using an acceptance radius R_J. To explain the definition of TP, FN and FP, let us assume that we have a theoretical wavenumber $k_{rm}^{theo}[\nu]$ and an estimated wavenumber $\widehat{k_r}[\nu]$:

- if $[k_{rm}^{theo}[\nu] - R_J, k_{rm}^{theo}[\nu] + R_J]$ contains a single estimated mode $\widehat{k_r}[\nu]$, then $\widehat{k_r}[\nu]$ is a TP;
- if $[k_{rm}^{theo}[\nu] - R_J, k_{rm}^{theo}[\nu] + R_J]$ contains several estimated modes, then the closest $\widehat{k_r}[\nu]$ from $k_{rm}^{theo}[\nu]$ is a TP while the others are FP (it is implicitely assumed that R_J is smaller than half of the smallest distance between all theoretical modes, i.e. the acceptance radii do not intercept);
- if there is no estimated mode $\widehat{k_r}[\nu]$ such that $|k_{rm}^{theo}[\nu] - \widehat{k_r}[\nu]| \leq R_J$ then $k_{rm}^{theo}[\nu]$ is a FN.

Mathematically, the Jaccard's index J_I is first defined

$$J_I = \frac{\mathrm{TP}}{\mathrm{TP} + \mathrm{FP} + \mathrm{FN}} \tag{18}$$

and leads to the definition of the Jaccard distance

$$D_J = 1 - J_I \tag{19}$$

which is such that $0 < D_J < 1$. Note that $D_J = 0$ means that $\mathrm{TP} = 1$ and $\mathrm{FP} = \mathrm{FN} = 0$. On the other hand $D_J = 1$ means that $\mathrm{TP} = 0$, while $D_J \gg 0$ means that FP and/or FN are much larger than TP.

The relevance of the Jaccard distance is illustrated using data simulated in our Pekeris waveguide example. For the sake of simplicity, wavenumbers are estimated using a classical OMP method. OMP is an iterative algorithm, selecting a new wavenumber at each iteration. Two stopping criteria are classically

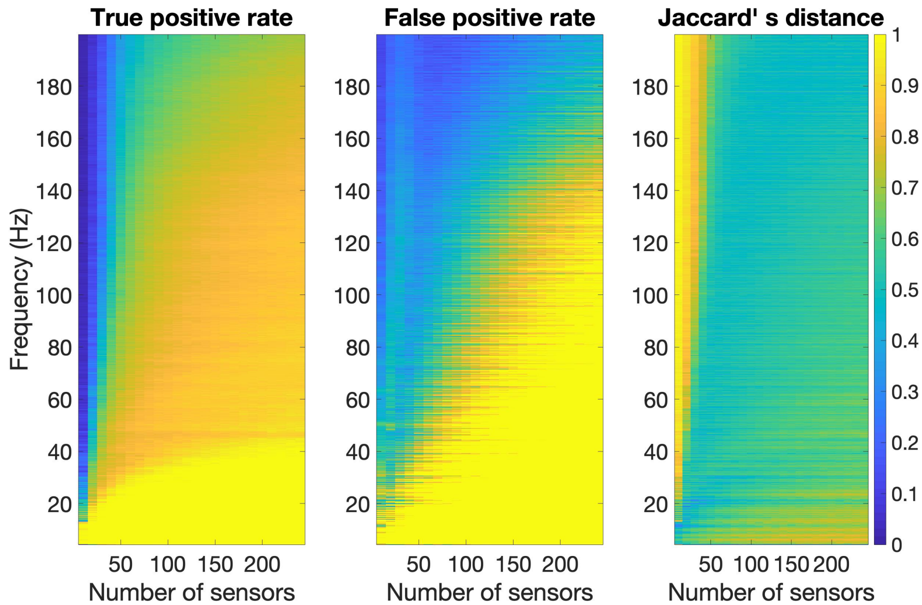

Fig. 3. Performance of the estimation of modal wavenumbers in a simulated Pekeris waveguide using OMP: TP (left), FP (middle) and D_J (right).

considered for this algorithm: it can stop either when the estimated reconstruction error drops below a given threshold or when the number of non-zero coefficients achieves a given number. This latter criterion is very convenient in our context, because the number of iterations is equivalent to the number of modes to be recovered. Although practical, this requires accurate prior information about the number of modes at each frequency. On the other hand, the stopping criterion based on the energy of the residual is less demanding in terms of prior information. This criterion is similar to what is used in the proposed method. It will thus be used to illustrate the interest of the Jaccard distance.

Estimation performance is illustrated in Fig. 3. The TP rate increases when the number of sensors increases (because more data makes the estimation easier), and increases when the frequency decreases (because modal density decreases which also facilitates the estimation). On the other hand, the FP rate is high at very low frequencies (because the number of modes is very low, and thus a single false positive drastically increases the FP rate). The FP rate also tends to increase with the number of sensors. This is due to the chosen stopping criterion which implies an increasing number of iterations in OMP, and thus increases the likeliness to make false positive mistakes.

Overall, the Jaccard distance D_J is consistent with the behavior of TP and FP. As an example, D_J is high (estimation performance is poor) when TP is small (e.g. for small number of sensors) and/or when FP is high (e.g. at very low frequencies). Also, when the sensor number is large enough, D_J is relatively constant, because TP and FP tend to compensate for each other. The Jaccard distance is thus a good metric to summarize global estimation performance and will be used in the following.

V. Application

In this section, the performance of the method is assessed on realistic simulations. The method is also applied on experimental marine data collected during the 2017 Seabed Characterization Experiment (SBCEX17). The considered applications focuses on low-frequency data ($f < 100$ Hz). In our context, this makes the number of modes relatively small (5 or less), which allows for modal estimation with a small number of sensors. This choice is consistent (and allows comparison) with previous modal estimation studies based on sparsity [12], [22], [28].

This section starts with a description of SBCEX17, whose context will be used to define the simulated environment.

A. SBCEX17

The SBCEX17 was dedicated to the understanding of sound propagation in fine-grained sediment. It was a multi-year, multi-institutional and multi-disciplinary effort which took place on the New England Mud Patch (NEMP). The NEMP is located about 100 km south of Cape Cod. The area is characterized by a relatively flat bathymetry (water depth $D \sim$ 70–75 m) and a thick upper sediment layer of mud.

A preliminary environmental survey was conducted in 2015. It notably included an intensive coring effort, as well as a high-resolution seismic survey. The main experiment took place in March-April 2017. It involved three research vessels, and many acoustic sources and receivers were deployed, covering frequencies from $\sim$ 10 Hz to 10 kHz. A previous special issue of the IEEE Journal of Oceanic Engineering is dedicated to SBCEX17. Its editorial introduction [23] provides a succint overview of SBCEX17.

B. Experimental context

The SBCEX data was collected on a long HLA (aperture $\sim$ 1 km). The considered source is a Combustive Sound Source deployed at 18:38 UTC on March 18 2017 at CSS station 29, located at (40.4983N, 70.5842W). The source signal is a powerful broadband impulse followed by several secondary impulses called bubble pulses [44]. Note that here, the specific source waveform does not matter as long as the source signal to noise ratio (SNR) is good enough in the frequency band of interest. The receiving system is a 64 element HLA with a horizontal aperture of 1016 m deployed by the Norwegian Defence Research Establishment (FFI). The array orientation was roughly West-East, and the positions of the hydrophones at the HLA extremities are (40.4984N, 70.4677W) and (40.4983N, 70.4557W). The hydrophone spacing along the array is not uniform. The array elements have approximately logarithmic spacing (from 0.8 m to 72 m), with a symmetry around the array center and a higher density in the middle of the array. The specific source/array configuration has been chosen so that the source is in the endfire direction, and the distance between the source and the HLA is about 10 km. Note that in this context, the range variability along the HLA induced by the $1/\sqrt{r}$ term in Eq. (1) is negligible and can be ignored.

C. Simulation framework

First, the performance of the method is assessed using simulated data that mimics the experimental context. The environment is modeled using results from an inversion study performed using the HLA data [45]. The environment is modeled as follows:

- water column: depth $D = 65$ m, sound speed gradient from 1468 m/s at the top of the layer to 1469 m/s at the bottom;
- sediment layer: thickness $h = 5$ m, sound speed $c_{\text{sed}} = 1500$ m/s, density $\rho_{\text{sed}} = 1.6$ g/cm^3, attenuation $\alpha_{\text{sed}} = 0.1$ dB/λ;
- basement: $c_{\text{bas}} = 1700$ m/s, density $\rho_{\text{bas}} = 2.0$ g/cm^3, attenuation $\alpha_{\text{sed}} = 0.2$ dB/λ.

Acoustic propagation is simulated in this environment over 0-100 Hz using the normal mode code ORCA [46] with a frequency bin size of 100 Hz, which led to simulation of 200 frequencies. The environmental impulse response along the array is simulated in the range-frequency domain for a source at $r = 10$ km in the endfire direction. The array configuration mimics the experimental geometry. A bi-dimensional (2D) Gaussian white noise is added to the impulse response in the range-frequency domain, and the signal to noise ratio (SNR) is evaluated as the power of the (2D) range-frequency impulse response divided by the power of the (2D) range-frequency noise. Speed correction (see Sec. IV-A) is then applied with $c_{\text{min}} = 1468$ m/s. Finally, f-k diagrams are computed using four different methods:

1) OMP: a traditional OMP algorithm;
2) SoBaP: a soft Bayesian Pursuit method that uses the dispersion relation to relate wavenumbers from one frequency to the next [22];
3) COMP: a grid-free OMP algorithm that uses gradient descent (COMP: Continuous OMP);
4) CPOMP: the method proposed in this article (CPOMP: Continuous and Physics-based OMP, i.e. which uses the dispersion relation).

The methods OMP, SoBaP and COMP have been chosen as representative of the state-of-the-art. Note that OMP and COMP have been implemented here using the mode number as a stopping criterion (i.e. at frequency f, each algorithm looks for $M(f)$ wavenumbers). This gives them a strong advantage over the proposed method, which automatically determines the mode number. For CPOMP, we set $\beta_0 = 0.001$, $\beta_\infty = 0.5$ and $\xi = 10^{-3}$.

Beside, all the methods considered here rely on the construction of the dictionary $\mathbf{D}$ (see Sec.III-A). To construct this dictionary, one needs to sample the wavenumber axis with N elements. This is done by choosing a grid size and a maximum wavenumber value of interest. The grid size is defined as one fifth of the smallest value between 2 propagating modes over the frequency band of interest. Further, the maximum wavenumber value is computed considering the Nyquist theorem applied to the maximum space between two consecutive sensor (here $\Delta_k = 5.10^{-4}$ rad/m and $\kappa_n = -0.09$ rad/m).

D. Performance study

A first set of simulations studies the impact of the number of sensors on the f-k diagram estimation for a given SNR (12 dB). For a given number of sensors, sensors are randomly selected, except for the two sensors at the extremities of the HLA which are always selected (these two sensors are on both ends of the HLA so that total aperture of the array is always the same). The obtained performance is shown in Fig. 4 for 2 different frequency bands: 0–50 Hz and 50–100 Hz. Clearly, performance increases with number of sensors for all the methods, and the proposed method (CPOMP) outperforms the state of the art. Performance gain is minimal in the 0–50 Hz band, because most methods (OMP, COMP, CPOMP) provide satisfactory results. However, at higher frequencies where more modes are propagating, the gains of the proposed method becomes evident, for all number of sensors. As an example, with 40 sensors, CPOMP has $D_J < 0.1$. This corresponds to an excellent f-k diagram recovery, as is illustrated at the end of this subsection. Interestingly, SoBaP which is supposed to be the most advanced of the state-of-the-art methods is the one with the worst performance. This is because SoBaP has been developed for data without speed correction. Although the SoBaP dispersion relation has been modified here to take into account the corrected dispersion relation, this is clearly not enough to correctly track wavenumbers. It is likely possible to further modify SoBaP to regain performance, but this is beyond the present scope.

A second set of simulations studies the impact of SNR for a given number of sensors (32), and for SNR from 0 dB to 12 dB. Again, for a given simulation, sensor selection is random but for the HLA extremities which are always used. Results are shown in Fig. 5. Performance naturally increases as SNR increases for all the methods. Once again, CPOMP outperforms all the other methods, and SoBaP exhibits poor performance. In particular, CPOMP provides very satisfactory f-k reconstruction ($D_J < 0.1$) for SNR > 5 dB. Also, both in Figs. 4 and 5, the performance gain of COMP with respect to OMP is relatively small, while the performance gain of CPOMP with respect to COMP is more significant. This

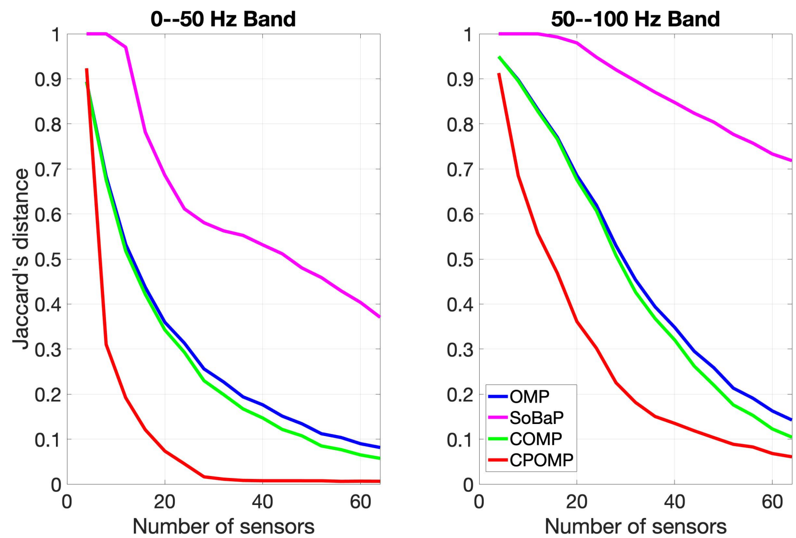

Fig. 4. Jaccard's distance as a function of the number of sensors for a SNR of 12 dB.

demonstrates the importance of including physics (the dispersion relation) at the core of any grid-free CS method.

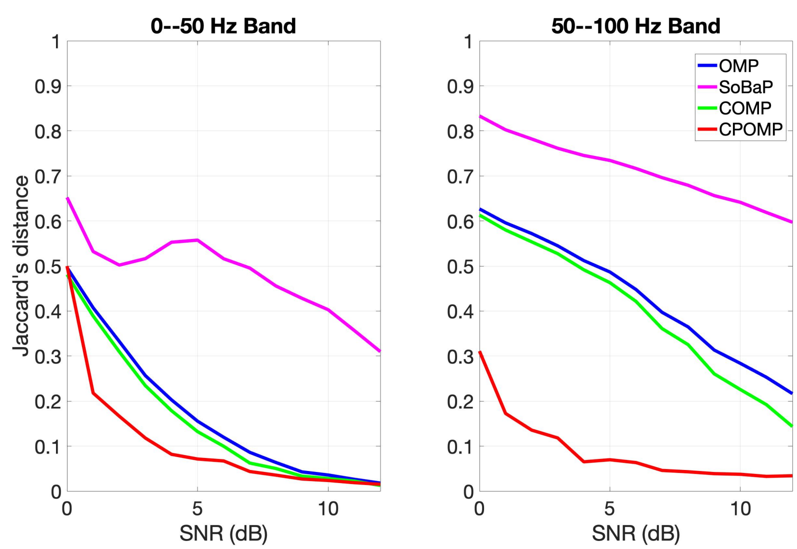

Fig. 5. Jaccard's distance as a function of the SNR - using 32 sensors

The Jaccard distance D_J fully characterizes the performance of the four methods. However, it is difficult to relate D_J values to an actual wavenumber tracking result. To illustrate the performance associated to specific D_J values, an example of wavenumber estimation with 40 sensors and $\mathrm{SNR} = 12$ dB is illustrated in Fig. 6. One can see that all the methods with $D_J < 0.3$ provide good results. The main advantage of CPOMP ($D_J < 0.1$) is a drastic reduction of false alarm. Further, wavenumber estimation results are also shown for 10 sensors and the same $\mathrm{SNR} = 12$ dB. The results of OMP and SoBaP are really poor ($D_J > 0.8$) and not shown here. However, Fig. 6 presents the estimation result for COMP ($D_J = 0.8$) and CPOMP ($D_J \simeq 0.7$). One can see that COMP suffers both from false alarms and missed detections. The performance of CPOMP are much better, with a clear reduction of false alarms.

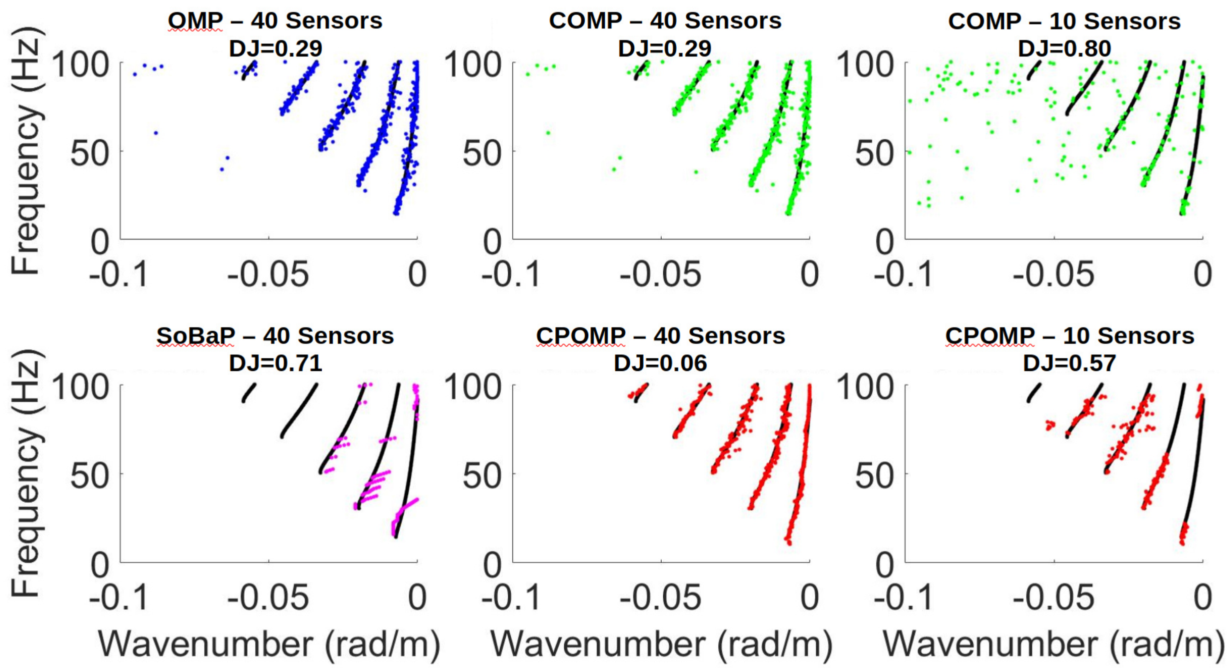

Fig. 6. (black) Theoretical wavenumbers, (blue) recovery with OMP, (purple) recovery with SoBaP, (green) recovery with COMP, (red) recovery with CPOMP ($\mathrm{SNR} = 12$ dB)

E. Experimental results

The proposed method is now applied to the experimental CSS data described in Sec. V-B. Speed correction is first applied on the data using $c_{\min} = 1459\ m/s$, a value empirically determined to time-align the data along the array. Wavenumber estimation is then performed using CPOMP and COMP. The objective here is to exclusively compare the proposed method (CPOMP) to the best method of the state-of-the-art (COMP).

Wavenumbers are estimated using 10, 40 and 64 sensors. Experimental results are presented in Fig. 7. Since no perfect ground truth is available to assess the experimental performance, the CPOMP 64-sensor estimation is used as a reference (black dots in Fig. 7) to visually evaluate the results. One can see that

CPOMP is consistently better than COMP. With 40 sensors, CPOMP gives results that are comparable to the 64-sensor reference. This is consistent with the simulated study which shows that CPOMP performance is roughly constant between 40 and 64 sensors (see Fig. 4). Interestingly, CPOMP also provides a good wavenumber estimation using only 10 sensors, although the last mode is missed. On the other hand, the COMP estimation with 10 sensors suffers from the small number of sensors, which leads to a consequent number of false alarms.

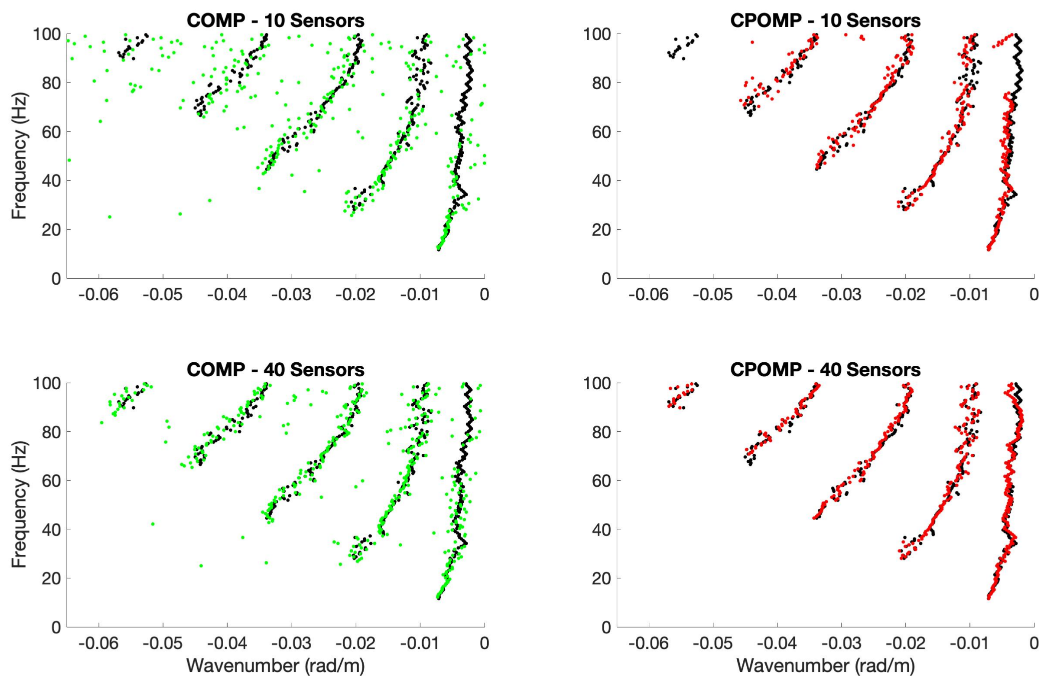

Fig. 7. (black) Recovery of CPOMP with 64 sensors, (green) recovery with COMP, (red) recovery with CPOMP

VI. Conclusion

The article presents a physics-based grid-free CS method to estimate modal wavenumber using a broadband source and a HLA with a small number of sensors. The method is based on three ideas. First of all, the method benefits from speed correction, so that a range-frequency signal can be conveniently sampled without wavenumber aliasing. Second, the method uses a grid-free framework to mitigate known CS drawbacks associated with basis mismatch. Last but not least, the method embeds physical information within the CS framework: it uses the dispersion relation (compensated for speed correction) to relate wavenumbers from one frequency to the other.

The proposed method has been benchmarked on simulations using the Jaccard distance as a performance metric. It was demonstrated that the method outperforms the state-of-the-art. Further, the method is experimentally validated on experimental data collected during SBCEX17. It notably allows a good estimation of modal wavenumbers from 0 to 100 Hz using as few as 10 sensors.

Although the proposed method works with a small number of sensors, it still requires a large horizontal aperture. As a result, a potential application for the method is modal estimation using synthetic aperture, as obtained using a fixed receiver and a moving source. This context is particularly appealing for geoacoustic inversion, where estimated modal wavenumbers can be used as an input to estimate the seafloor geoacoustic properties [8], [47]. Following the CS paradigm, the proposed method can be used to collect fewer samples, but exploiting them in a smarter way. This has practical consequences for ocean acoustics, since the production of man-made source signal underwater is now considered as pollution [48]. Reducing the number of samples (which is equivalent to the number of source signals in a synthetic aperture context) is an important perspective to reduce the noise footprint of ocean acoustic experiments.

ACKNOWLEDGMENT

This work was supported by the Delegation Generale de L'Armement (DGA), the Office of Naval Research (ONR), the ONR Global, the LABEX CeLyA (ANR-10-LABX-0060) of Université de Lyon, within the program "Investissements d'Avenir" (ANR-16-IDEX-0005) operated by the French National Research Agency (ANR).

REFERENCES

[1] G. R. Wilson, R. A. Koch, and P. J. Vidmar, “Matched mode localization,” *The Journal of the Acoustical Society of America*, vol. 84, no. 1, pp. 310–320, 1988.

[2] Y. Le Gall, F.-X. Socheleau, and J. Bonnel, “Performance analysis of single-receiver matched-mode localization,” *IEEE Journal of Oceanic Engineering*, vol. 44, no. 1, pp. 193–206, 2017.

[3] G. V. Frisk and J. F. Lynch, “Shallow water waveguide characterization using the Hankel transform,” *The Journal of the Acoustical Society of America*, vol. 76, no. 1, pp. 205–216, 1984.

[4] M. S. Ballard and K. M. Becker, “Inversion for range-dependent water column sound speed profiles on the New Jersey shelf using a linearized perturbative method,” *The Journal of the Acoustical Society of America*, vol. 127, no. 6, pp. 3411–3421, 2010.

[5] Ö. Yilmaz, *Seismic data analysis: Processing, inversion, and interpretation of seismic data*, ch. 1–2. No. 10, Society of Exploration Geophysicists (Tulsa), 2001.

[6] B. Nicolas, J. Mars, and J.-L. Lacoume, “Geoacoustical parameters estimation with impulsive and boat-noise sources,” *IEEE Journal of Oceanic Engineering*, vol. 28, no. 3, pp. 494–501, 2003.

[7] K. M. Becker and G. V. Frisk, “Evaluation of an autoregressive spectral estimator for modal wave number estimation in range-dependent shallow water waveguides,” *The Journal of the Acoustical Society of America*, vol. 120, no. 3, pp. 1423–1434, 2006.

[8] M. S. Ballard, K. M. Becker, and J. A. Goff, “Geoacoustic inversion for the New Jersey shelf: 3-D sediment model,” *IEEE Journal of Oceanic Engineering*, vol. 35, no. 1, pp. 28–42, 2010.

[9] E. J. Candès and M. B. Wakin, “An introduction to compressive sampling,” *IEEE Signal Processing Magazine*, vol. 25, no. 2, pp. 21–30, 2008.

[10] N. Chapman and I. Barrodale, “Deconvolution of marine seismic data using the l_1 norm,” *Geophysical Journal International*, vol. 72, no. 1, pp. 93–100, 1983.

[11] P. Gerstoft, A. Xenaki, and C. F. Mecklenbräuker, “Single and multiple snapshot compressive beamforming,” *arXiv preprint arXiv:1503.02339*, 2015.

[12] F. Le Courtois and J. Bonnel, “Compressed sensing for wideband wavenumber tracking in dispersive shallow water,” *The Journal of the Acoustical Society of America*, vol. 138, no. 2, pp. 575–583, 2015.

[13] J. B. Harley and J. M. Moura, “Dispersion curve recovery with orthogonal matching pursuit,” *The Journal of the Acoustical Society of America*, vol. 137, no. 1, pp. EL1–EL7, 2015.

[14] S. Sabeti, C. A. Leckey, L. De Marchi, and J. B. Harley, “Sparse wavenumber recovery and prediction of anisotropic guided waves in composites: a comparative study,” *IEEE Transactions on Ultrasonics, Ferroelectrics, and Frequency Control*, vol. 66, no. 8, pp. 1352–1363, 2019.

[15] P. Gerstoft, C. Mecklenbräuker, W. Seong, and M. Bianco, “Introduction to special issue on compressive sensing in acoustics,” *The Journal of the Acoustical Society of America*, vol. 143, no. 6, pp. 3731–3731, 2018.

[16] M. F. Duarte and R. G. Baraniuk, “Spectral compressive sensing,” *Applied and Computational Harmonic Analysis*, vol. 35, no. 1, pp. 111–129, 2013.

[17] K. C. Knudson, J. Yates, A. Huk, and J. W. Pillow, “Inferring sparse representations of continuous signals with continuous orthogonal matching pursuit,” in *Advances in Neural Information Processing Systems*, pp. 1215–1223, 2014.

[18] Q. Denoyelle, *Theoretical and Numerical Analysis of Super-Resolution Without Grid.* PhD thesis, Paris Sciences et Lettres, 2018.

[19] A. Xenaki and P. Gerstoft, "Grid-free compressive beamforming," *The Journal of the Acoustical Society of America*, vol. 137, no. 4, pp. 1923–1935, 2015.

[20] Y. Park, P. Gerstoft, and W. Seong, "Grid-free compressive mode extraction," *The Journal of the Acoustical Society of America*, vol. 145, no. 3, pp. 1427–1442, 2019.

[21] T. Paviet-Salomon, C. Dorffer, J. Bonnel, B. Nicolas, T. Chonavel, and A. Drémeau, "Dispersive grid-free orthogonal matching pursuit for modal estimation in ocean acoustics," in *ICASSP 2020-2020 IEEE International Conference on Acoustics, Speech and Signal Processing (ICASSP)*, pp. 4602–4606, IEEE, 2020.

[22] A. Drémeau, F. Le Courtois, and J. Bonnel, "Reconstruction of dispersion curves in the frequency-wavenumber domain using compressed sensing on a random array," *IEEE Journal of Oceanic Engineering*, vol. 42, no. 4, pp. 914–922, 2017.

[23] P. S. Wilson, D. P. Knobles, and T. B. Neilsen, "Guest editorial an overview of the seabed characterization experiment," *IEEE Journal of Oceanic Engineering*, vol. 45, no. 1, pp. 1–13, 2020.

[24] J. Belcourt, C. W. Holland, S. E. Dosso, J. Dettmer, and J. A. Goff, "Depth-dependent geoacoustic inferences with dispersion at the new england mud patch via reflection coefficient inversion," *IEEE Journal of Oceanic Engineering*, vol. 45, no. 1, pp. 69–91, 2019.

[25] M. S. Ballard, K. M. Lee, A. R. McNeese, P. S. Wilson, J. D. Chaytor, J. A. Goff, and A. H. Reed, "In situ measurements of compressional wave speed during gravity coring operations in the new england mud patch," *IEEE Journal of Oceanic Engineering*, vol. 45, no. 1, pp. 26–38, 2019.

[26] J. Bonnel, S. Dosso, J. Goff, Y. Lin, J. Miller, G. Potty, P. Wilson, and D. Knobles, "Trans-dimensional geoacoustic inversion using prior information on range-dependent seabed layering," *IEEE Journal of Oceanic Engineering*, 2021. in press (DOI: 10.1109/JOE.2021.3062719).

[27] F. B. Jensen, W. A. Kuperman, M. B. Porter, and H. Schmidt, *Computational Ocean Acoustics*, ch. 5,10. Springer Science & Business Media, 2011.

[28] H. Niu, P. Gerstoft, E. Ozanich, Z. Li, R. Zhang, Z. Gong, and H. Wang, "Block sparse bayesian learning for broadband mode extraction in shallow water from a vertical array," *The Journal of the Acoustical Society of America*, vol. 147, no. 6, pp. 3729–3739, 2020.

[29] S. S. Chen, D. L. Donoho, and M. A. Saunders, "Atomic decomposition by basis pursuit," *SIAM review*, vol. 43, no. 1, pp. 129–159, 2001.

[30] Y. C. Pati, R. Rezaiifar, and P. S. Krishnaprasad, "Orthogonal matching pursuit: Recursive function approximation with applications to wavelet decomposition," in *Proceedings of 27th Asilomar Conference on Signals, Systems and Computers*, pp. 40–44, IEEE, 1993.

[31] B. A. Olshausen and D. J. Field, "Sparse coding with an overcomplete basis set: A strategy employed by v1?," *Vision Research*, vol. 37, no. 23, pp. 3311–3325, 1997.

[32] C. Fevotte and S. J. Godsill, "A bayesian approach for blind separation of sparse sources," *IEEE Transactions on Audio, Speech, and Language Processing*, vol. 14, no. 6, pp. 2174–2188, 2006.

[33] Y. Chi, L. L. Scharf, A. Pezeshki, and A. R. Calderbank, "Sensitivity to basis mismatch in compressed sensing," *IEEE Transactions on Signal Processing*, vol. 59, no. 5, pp. 2182–2195, 2011.

[34] E. J. Candès and C. Fernandez-Granda, "Towards a mathematical theory of super-resolution," *Communications on Pure and Applied Mathematics*, vol. 67, no. 6, pp. 906–956, 2014.

[35] M. Grant and S. Boyd, "CVX: Matlab software for disciplined convex programming, version 2.1," 2014.

[36] C. Ekanadham, D. Tranchina, and E. P. Simoncelli, "Recovery of sparse translation-invariant signals with continuous basis pursuit," *IEEE Transactions on Signal Processing*, vol. 59, no. 10, pp. 4735–4744, 2011.

[37] P. Chen, Z. Cao, Z. Chen, and C. Yu, "Sparse off-grid doa estimation method with unknown mutual coupling effect," *Digital Signal Processing*, vol. 90, pp. 1–9, 2019.

[38] D. P. Bertsekas, "Nonlinear programming," *Journal of the Operational Research Society*, vol. 48, no. 3, pp. 334–334, 1997.

[39] S. L. Freire and T. J. Ulrych, "Application of singular value decomposition to vertical seismic profiling," *Geophysics*, vol. 53, no. 6, pp. 778–785, 1988.

[40] G. Duncan and G. Beresford, "Median filter behaviour with seismic data 1," *Geophysical Prospecting*, vol. 43, no. 3, pp. 329–345, 1995.

[41] M. Nardin, F. Glangeaud, and D. Mauuary, "1-200 Hz wave propagation in shallow water," in *IEEE Oceanic Engineering Society. OCEANS'98. Conference Proceedings (Cat. No. 98CH36259)*, vol. 1, pp. 390–394, IEEE, 1998.

[42] P. Jaccard, "Étude comparative de la distribution florale dans une portion des Alpes et des Jura," *Bull Soc Vaudoise Sci Nat*, vol. 37, pp. 547–579, 1901.

[43] J. C. Gower and M. J. Warrens, "Similarity, dissimilarity, and distance, measures of," *Wiley StatsRef: Statistics Reference Online*, pp. 1–11, 2014.

[44] A. R. McNeese, P. S. Wilson, J. D. Sagers, and D. P. Knobles, "An impulsive source with variable output and stable bandwidth for underwater acoustic experiments," *The Journal of the Acoustical Society of America*, vol. 136, no. 1, pp. EL8–EL12, 2014.

[45] D. Tollefsen, S. E. Dosso, and D. P. Knobles, "Ship-of-opportunity noise inversions for geoacoustic profiles of a layered mud-sand seabed," *IEEE Journal of Oceanic Engineering*, vol. 45, no. 1, pp. 189–200, 2019.

[46] E. K. Westwood, C. T. Tindle, and N. R. Chapman, "A normal mode model for acousto-elastic ocean environments," *The Journal of the Acoustical Society of America*, vol. 100, no. 6, pp. 3631–3645, 1996.

[47] G. V. Frisk, K. M. Becker, S. D. Rajan, C. J. Sellers, K. Von Der Heydt, C. M. Smith, and M. S. Ballard, "Modal mapping experiment and geoacoustic inversion using sonobuoys," *IEEE Journal of Oceanic Engineering*, vol. 40, no. 3, pp. 607–620, 2014.

[48] C. M. Duarte, L. Chapuis, S. P. Collin, D. P. Costa, R. P. Devassy, V. M. Eguiluz, C. Erbe, T. A. Gordon, B. S. Halpern, H. R. Harding, *et al.*, "The soundscape of the anthropocene ocean," *Science*, vol. 371, no. 6529, 2021.